

# Programmable Periodicity of Quantum Dot Arrays with DNA Origami Nanotubes

Hieu Bui,<sup>†</sup> Craig Onodera,<sup>‡</sup> Carson Kidwell,<sup>‡</sup> YerPeng Tan,<sup>‡</sup> Elton Graugnard,<sup>‡</sup> Wan Kuang,<sup>†</sup> Jeunghoon Lee,<sup>§</sup> William B. Knowlton,<sup>†,‡</sup> Bernard Yurke,<sup>†,‡</sup> and William L. Hughes\*,<sup>†</sup>

<sup>†</sup>Department of Electrical and Computer Engineering, <sup>‡</sup>Department of Materials Science and Engineering, and

<sup>§</sup>Department of Chemistry and Biochemistry, Boise State University, Boise Idaho 83725

**ABSTRACT** To fabricate quantum dot arrays with programmable periodicity, functionalized DNA origami nanotubes were developed. Selected DNA staple strands were biotin-labeled to form periodic binding sites for streptavidin-conjugated quantum dots. Successful formation of arrays with periods of 43 and 71 nm demonstrates precise, programmable, large-scale nanoparticle patterning; however, limitations in array periodicity were also observed. Statistical analysis of AFM images revealed evidence for steric hindrance or site bridging that limited the minimum array periodicity.

**KEYWORDS** DNA, origami, nanoparticles, quantum dot, self-assembly, periodic

The ability to precisely pattern nanoparticles is essential for realizing the potential of nanoelectronic and nanoplasmionic devices.<sup>1–3</sup> Over the past decade, DNA oligonucleotides have been programmed to aggregate,<sup>4,5</sup> crystallize,<sup>6,7</sup> and self-assemble into spatially discrete assemblies<sup>8–13</sup> and linear arrays.<sup>14–16</sup> DNA nanotechnology offers a compelling approach toward programmable nanoparticle patterning.<sup>17–20</sup> By implementing basic design rules, DNA can be used to form complex nanostructures using the methods of either tiled DNA motifs or DNA origami.<sup>21–27</sup> When functionalized, these nanostructures can serve as two-dimensional<sup>28–36</sup> and three-dimensional<sup>37</sup> nanoparticle scaffolds. Several groups have reported successful attachment of semiconductor quantum dots (QDs) to functionalized DNA.<sup>10,33,38</sup> Sharma et al. recently reported the fabrication of periodic QD arrays formed by tiling DNA motifs.<sup>33</sup> While tiling methods have the ability to create highly ordered complex arrays, they tend to create continuous sheets; the boundaries of which are not well controlled.

Presented here is a method of fabricating nanoparticle arrays with controlled periodicity using three-dimensional, six-helix DNA origami nanotubes. DNA origami nanotubes of predetermined dimensions were used to precisely arrange nanoparticles by incorporating binding sites along the axis of the nanotube using biotin-labeled staple strands. The unique sequence of each staple strand permits precise spatial control and modular design of periodic or aperiodic binding sites. The three-dimensional DNA origami nanotubes provide a rigid structure for nanoparticle attachment in solution. Additionally, the extension of the DNA nanotubes into networks via dimerization, polymerization, or

branching offers controlled fabrication of more complex nanoparticle structures.

The DNA origami nanotubes used in this research were designed using the principles reported by Mathieu et al.<sup>39</sup> and Douglas et al.<sup>40</sup> where the single-stranded M13mp18 DNA molecule was folded into a six-helix nanotube bundle using the DNA origami method developed by Rothemund.<sup>25</sup> The design reported here uses 170 unique staple strands to fold the single-stranded M13mp18 scaffold, resulting in DNA nanotubes with blunt ends that do not dimerize. The nanotube design is illustrated and described in detail in the Supporting Information S1. Staple strands include 9 strands with 69 nucleotides, 9 strands with 35 nucleotides, and 152 strands with 42 nucleotides (see Supporting Information S2). The DNA nanotubes were designed to be 412 nm in length and 6 nm in diameter. To incorporate nanoparticle binding sites, prior to nanotube synthesis, selected staple strands were extended with a 2.2 nm tether consisting of 5 thymine nucleotides and modified with biotin at the 3' end. The resulting DNA nanotubes possessed precisely spaced biotin binding sites for controlled positioning of streptavidin-conjugated nanoparticles along the length of the nanotube (see Supporting Information S3).

To test controlled nanoparticle patterning, four distinct DNA nanotubes were synthesized with evenly spaced binding sites designed to attach 5, 9, 15, or 29 streptavidin-conjugated nanoparticles to form arrays with periodicities of 71, 43, 29, or 14 nm, respectively. The biotin-labeled DNA nanotubes were designed by functionalizing the appropriate staple strands, as described above. The nanotubes were synthesized by combining M13mp18 viral DNA (New England Biolabs) with unmodified and biotin-labeled staple strands (Integrated DNA Technologies) in a molar ratio of 1:10:10 in a solution of 1 × TAE, Mg<sup>2+</sup> (40 mM tris, 20 mM acetic acid, 2 mM ethylenediaminetetraacetic acid (EDTA),

\* To whom correspondence should be addressed: WillHughes@BoiseState.edu.

Received for review: 03/27/2010

Published on Web: 08/03/2010

and 12.5 mM magnesium acetate; pH 8.0). TAE, magnesium acetate tetrahydrate, and laboratory grade water (Milli-Q Water, Millipore) were purchased from Sigma Aldrich. All DNA strands were used without further purification. To form nanotubes, the DNA solution was thermally annealed at 90 °C for 20 min, then cooled to 20 °C at ~1 °C per minute using a thermal cycler (Mastercycler, Eppendorf). After the nanotubes were synthesized, the solution was centrifuged using a centrifugal filter (100 000 molecular weight cut off) at 500 g for 15 min to remove excess staple strands and small, unbound DNA fragments.

Successful formation of biotin-labeled DNA nanotubes was confirmed via atomic force microscopy (AFM). During sample preparation, 5  $\mu$ L of DNA nanotube solution was dispersed onto freshly cleaved V-4 grade mica with 20  $\mu$ L of 1  $\times$  TAE, Mg<sup>2+</sup> buffer and allowed to adsorb onto the surface for 5 min. Then, the surface was washed with Milli-Q water and dried with compressed air. Imaging of functionalized nanotubes was performed using AFM (Multimode Picoforce with a Nanoscope IV controller, Veeco Metrology) under ambient conditions in AC mode using silicon cantilever-based tips (PPP-NCH, Nanosensors). Cantilevers had a nominal spring constant of 42 N/m with a range of 10–130 N/m. To validate the linearity, stability, and accuracy of the piezoelectric scanner, the AFM was calibrated using (1) a surface topography reference (STR) with precision fabricated silicon dioxide rectangular features (VLSI Standards), and (2) the atomic step height of freshly cleaved, ZYH grade, highly ordered pyrolytic graphite (HOPG, Veeco Metrology) (see Supporting Information S4).

Figure 1 shows DNA origami nanotubes with nine biotin binding sites as synthesized (a–e), after functionalization with streptavidin (f–j), and after functionalization with streptavidin-conjugated quantum dots (k–o). Figure 1a illustrates the biotin-labeled nanotube structure, while panels b and c show low- and high-magnification AFM height images, respectively. The dashed line in panel c indicates the location of the cross-sectional height profile in panel d. From this profile, a nanotube height of ~2.6 nm is measured. When measured under various imaging conditions, the mean nanotube height ranged from  $3.5 \pm 0.1$  to  $1.7 \pm 0.4$  nm (see Supporting Information S5). The axial profile shown in panel e emphasizes relative height variations along the nanotube length (see Supporting Information S6). The mean nanotube length was measured to be  $436 \pm 14$  nm from 100 samples and was independent of the imaging conditions. The DNA origami nanotubes were designed to have a circular cross-section equivalent to 3 double helices (i.e., 6 nm)<sup>39</sup> with an expected length of 412 nm. While the nanotube length is in agreement with the expected value, the height is less than the expected diameter. According to Douglas et al., the diameter of DNA nanotubes with six helices was  $\sim 7 \pm 2$  nm using transmission electron microscopy (TEM).<sup>40</sup> Sources of deviation may include the nanotube collapsing onto the mica surface because of surface van

der Waals forces,<sup>41,42</sup> capillary effects encountered when imaging in ambient conditions,<sup>41</sup> and compressive forces during AFM imaging<sup>43–45</sup> (see Supporting Information S5). For example, reduced AFM height profiles for soft biological samples have been reported in multiple studies.<sup>41,46,47</sup>

Once biotin-labeled DNA nanotubes were verified via AFM, the accessibility and reactivity of the biotin attachment sites were tested by combining a 1 nM solution of biotin-labeled nanotubes with pure, lyophilized streptavidin purchased from Sigma Aldrich that was resuspended in Milli-Q water at 200 nM. The components were allowed to react for 2 h at room temperature. The reacted nanotubes were dispersed onto a freshly cleaved mica surface and dried as described above. Figure 1f illustrates the biotin-labeled DNA nanotubes with attached streptavidin. The successful attachment of nine streptavidin molecules is clearly observed by comparison of the high-magnification AFM images without streptavidin in panel c and with streptavidin in panel h. The cross-sectional profile in panel i, obtained at an apparent streptavidin site, reveals a height increase of ~0.5 nm relative to the nanotube shown in panel d. The axial profile in panel j clearly displays nine peaks with a periodicity of 45 nm, very close to the expected value of 43 nm.

While the measured height increase at a streptavidin site was ~0.5 nm, the mean height of free streptavidin, dispersed onto freshly cleaved mica, was measured to range from  $2.3 \pm 0.5$  to  $0.7 \pm 0.2$  nm under various imaging conditions (see Supporting Information S5). Although X-ray analysis of dehydrated streptavidin crystals indicated a thickness of 4.6 nm,<sup>48–51</sup> Weisenhorn et al. imaged streptavidin under different AFM contact forces and demonstrated that the maximum height varied between 1.12, 0.65, and 0.25 nm at 30, 60, and 150 pN, respectively.<sup>44</sup> Thus, the streptavidin heights measured here are consistent with previous studies.

CdSe/ZnS core/shell streptavidin-conjugated quantum dots (Qdot 585, Invitrogen), hereafter referred to as quantum dots, with an average diameter of 15–20 nm were chosen to test nanoparticle attachment. To ensure a high attachment yield, a 1 nM solution of functionalized DNA nanotubes was combined at room temperature with a 200 nM solution of quantum dots for 2 h. The reacted DNA nanotubes with attached quantum dots were dispersed onto a mica surface and dried as described above. Figure 1k illustrates the attachment of the quantum dots to the biotin-labeled DNA nanotubes. Figure 1l,m respectively shows low- and high-magnification AFM height images of the DNA nanotubes with attached quantum dots. When compared to panels c and h, quantum dots attach to biotin-labeled DNA nanotubes with the same periodic spacing. Additionally, the cross-sectional profile across an apparent quantum dot in panel n yields a height of 5.5 nm, nearly twice the measured height of the nanotube with no attached particles. The mean height of free quantum dots, dispersed onto freshly cleaved mica, was measured to range from  $5.5 \pm 0.6$  to  $4.7 \pm 0.7$  nm

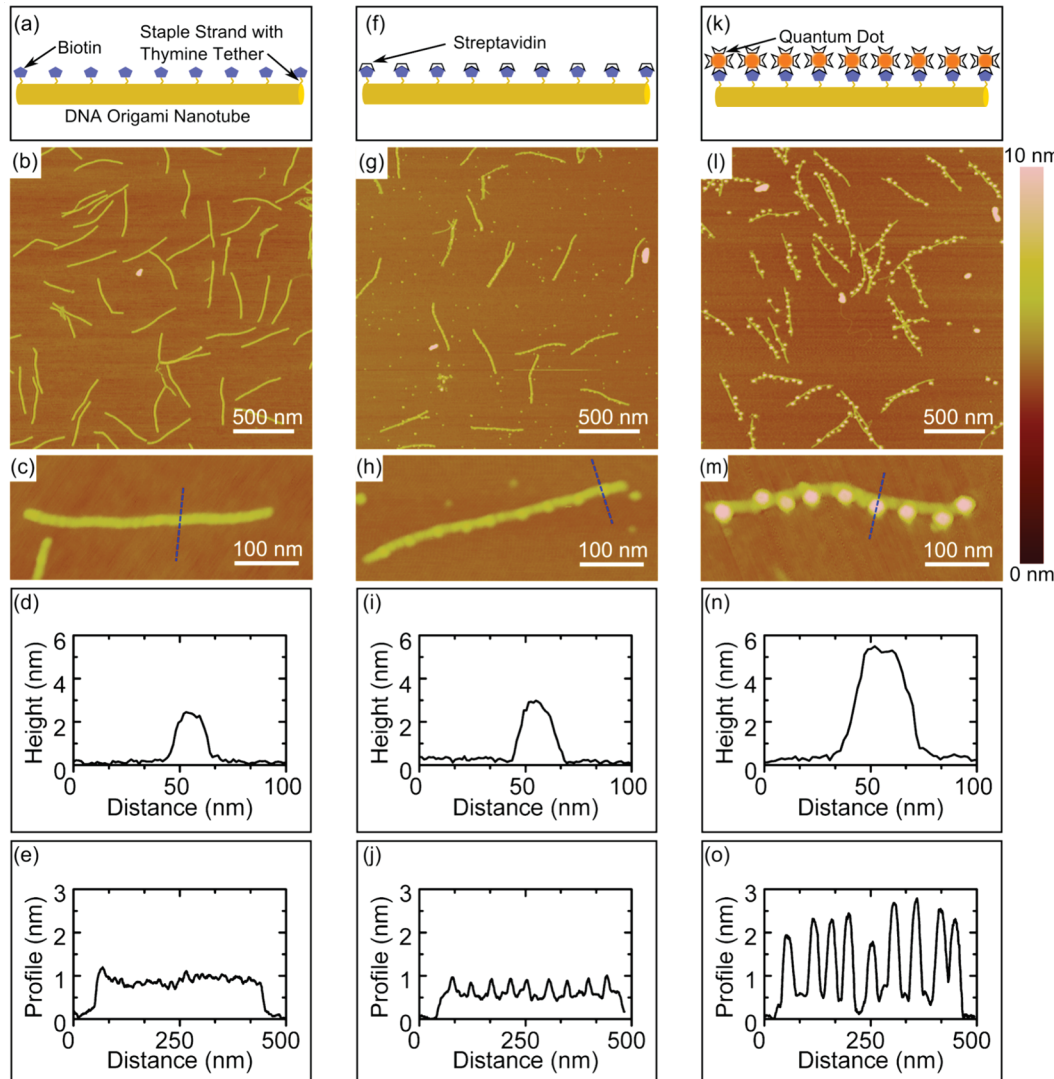


**FIGURE 1.** Schematics, AFM images at low magnification (upper) and high magnification (lower), and cross-sectional (upper) and axial (lower) height profiles of functionalized DNA origami nanotubes with nine biotin binding sites with (a–e) no attached nanoparticles; (f–j) attached streptavidin; and (k–o) attached streptavidin-conjugated quantum dots. The dashed lines in the high-magnification AFM images indicate the location of the cross-sectional profiles. Axial profiles represent the average of multiple profiles across the width of the nanotube (see Supporting Information S6).

under various imaging conditions (see Supporting Information S5). Although the diameter of the streptavidin-conjugated quantum dots is  $\sim 20$  nm in solution according to manufacturer specifications, the AFM height measurements of the dehydrated quantum dots correspond to the approximate diameter of the CdSe/ZnS quantum dot core/shell, as measured by TEM (see Supporting Information S7). Thus, with the chosen AFM imaging conditions the dehydrated streptavidin and polymer layer contributed very little to the measured height of the conjugated nanoparticle. The axial profile in panel o again shows nine equally spaced peaks with a periodicity of 49 nm.

To illustrate the flexibility of the design and confirm control over nanoparticle attachment, functionalized DNA nanotubes were synthesized with 5, 9, 15, and 29 biotin attachment sites to enable the formation of quantum dot

arrays with periodicities of 71, 43, 29, and 14 nm, respectively. These nanotubes were reacted with quantum dots and dispersed onto mica substrates as in the manner described above. Figure 2 shows high-magnification height images of quantum dots attached to DNA nanotubes with (a) 5, (b) 9, (c) 15, and (d) 29 biotin binding sites. Successful attachment to each biotin binding site was observed for nanotubes with 5 or 9 available sites; however, attached quantum dots were not observed at each site for nanotubes with 15 or 29 available sites. The average quantum dot spacings were measured to be approximately  $71 \pm 3$ ,  $49 \pm 4$ ,  $46 \pm 5$ , and  $31 \pm 4$  nm for nanotubes with 5, 9, 15, and 29 available biotin binding sites, respectively. The measured spacings for 5 and 9 binding sites agree well with the predicted periods of 71 and 43 nm. However, the arrays seen in Figure 2c,d formed with a reduced number of quantum dots and,

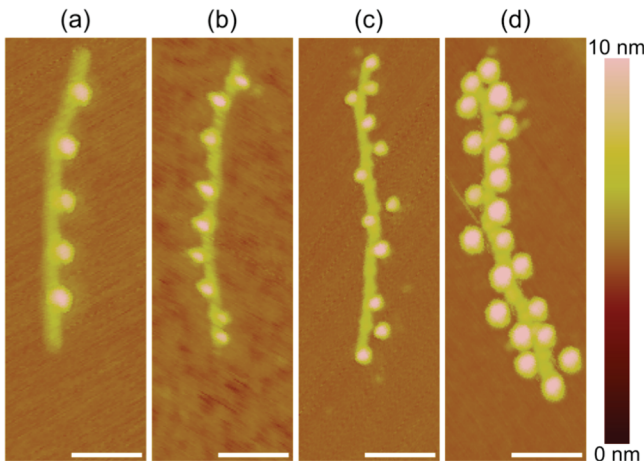


**FIGURE 2.** High-magnification AFM images of streptavidin-conjugated quantum dots attached to functionalized DNA origami nanotubes with (a) 5 binding sites, 71 nm period; (b) 9 binding sites, 43 nm period; (c) 15 binding sites, 29 nm period; and (d) 29 binding sites, 14 nm period. All scale bars are 100 nm. Note (c) and (d) have fewer attached quantum dots than available binding sites. In addition, the diameter of quantum dots varies between images because of variation in tip radii between scans.

consequently, a larger spacing than expected, that is, 29 and 14 nm, respectively. Additionally, successful attachment of 15 quantum dots to a DNA nanotube functionalized with 29 biotin binding sites was observed by TEM (see Supporting Information S7). The average quantum dot spacing was measured to be  $28 \pm 7$  nm, in agreement with the average spacing measured by AFM.

In Figure 2, only 10 quantum dots were attached to the nanotube with 15 available sites, and only 17 quantum dots were attached to the nanotube with 29 available sites. It is also noted that for the cases of 15 and 29 binding sites, the attached quantum dots alternate from one side of the DNA nanotube to the other with a greater frequency than for the cases of 5 or 9 binding sites. Several factors, hereafter referred to as binding obstructions, that may limit quantum dot attachment include (1) steric hindrance between quantum dots, (2) quantum dots bridging multiple biotin-labeled staple strands, (3) site poisoning of biotin-labeled staple strands by free streptavidin, (4) biotin-labeled staple strands that are missing their biotin modification, and (5) trapping of tethered biotin inside the DNA nanotube. Based on the design of the DNA nanotubes, 15 and 29 binding sites correspond to periodicities of 29 and 14 nm, respectively. AFM measurements of the center-to-center quantum dot separation show a minimum separation distance of 20 nm, which we interpret as the effective diameter of the quantum dots in solution (see Supporting Information S8). Thus, steric hindrance is expected for an array periodicity of 20 nm or less (e.g., 14 nm).

To further assess the degree of successful quantum dot attachment, Figure 3 shows histograms of the number of quantum dots attached to DNA nanotubes labeled with (a) 5, (b) 9, (c) 15, and (d) 29 biotin binding sites. The data for

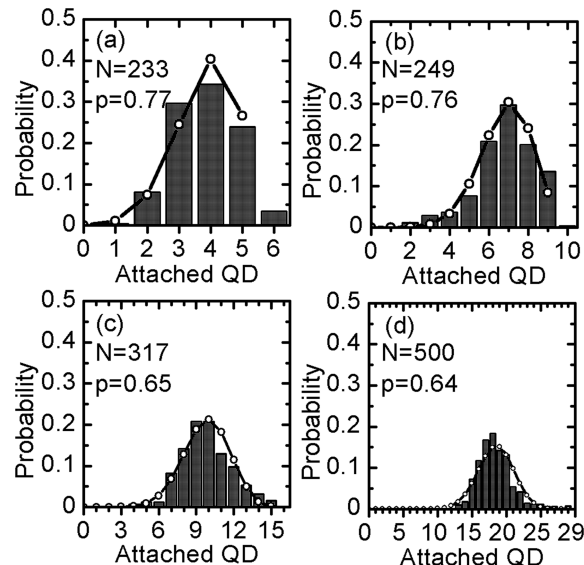


**FIGURE 3.** Histograms (bars) and calculated binomial distributions (lines) for the number of attached quantum dots for DNA nanotubes with (a) 5, (b) 9, (c) 15, and (d) 29 biotin binding sites. Data for each histogram were compiled from AFM image analysis for over 225 separate nanotubes, with the exact number,  $N$ , shown for each histogram. The average attachment probabilities,  $p$ , used to generate the calculated binomial distributions are indicated for each case.

the histograms were compiled from AFM image analysis for over 225 separate nanotubes for each case (see Supporting Information S9). For the cases of 5 and 9 available binding sites, the histograms are peaked at 4 and 7 successful attachments, very near the designed number of sites. However, in the cases of 15 and 29 available sites, the histograms are peaked at 10 and 17 successful attachments, confirming that attachment to each available binding site is much more likely for nanotubes functionalized with 5 or 9 binding sites than for those with 15 or 29. It is also noted that a small number of nanotubes appeared to have more attached quantum dots than available binding sites, which we attribute to coincidental alignment of a nanotube with full attachment and free quantum dots.

Assuming that quantum dot binding events occur with an equal average attachment probability for each site, the attachment histograms would be expected to follow a binomial distribution,  $P(m)$ , given by

$$P(m) = \frac{n!}{m!(n-m)!} p^m (1-p)^{n-m} \quad (1)$$

where  $n$  is the given number of available biotin binding sites per nanotube and  $m$  is the number of attached quantum dots per nanotube.<sup>52</sup> The average attachment probability,  $p$ , is given by

$$p = \frac{\sum \text{attached QD}}{\sum \text{available sites}} \quad (2)$$

where the numerator is the total number of attached quantum dots, and the denominator is the total number of available attachment sites. The average attachment probabilities were calculated using eq 2 from the histogram data to be 0.77, 0.76, 0.65, and 0.64 for 5, 9, 15, and 29 sites, respectively. For the case of 5 binding sites, the attachment probability for pure streptavidin was calculated from histogram data to be 0.79, only slightly higher than for quantum dot attachment (see Supporting Information S10). Similar attachment probabilities for pure streptavidin and quantum dots may indicate biotin-labeled staple strands are missing their biotin modification and/or tethered biotin is trapped inside the DNA nanotube. The solid lines in Figure 3 plot the calculated binomial distribution of eq 1 for each case. Overall, the calculated distributions follow the data well, confirming equal attachment probability per site. However, the histograms in Figure 3c,d display a slight shift toward lower attachment, providing some evidence for steric hindrance or site bridging.

For evidence of steric hindrance or bridging, the nearest-neighbor separation distances, projected along the nanotube axis, were measured for pairs of bound quantum dots (see Supporting Information S11). In the absence of steric hindrance or site bridging, the nearest-neighbor separation histograms would be expected to follow a geometric distribution peaked at the designed nanotube binding site periodicity. The geometric distribution,  $P(l)$ , of nearest-neighbor separations is given by

$$P(l) = p(1 - p)^{(l-1)} \quad (3)$$

where  $l$  is the integer number of periods between nearest-neighbors.<sup>52</sup> Histograms of the nearest-neighbor separations and the geometric distributions calculated using the average attachment probabilities  $p$  are shown in Figure 4 for each of the four cases. For each case, measured nearest-neighbor separation distances were normalized to represent the number of designed binding site periods between particles. The data were sorted into bins of width  $a$  centered on the  $n^{\text{th}}$  period, where  $a$  is the designed nanotube periodicity and  $n$  is an integer. Thus, nearest-neighbor separations of less than  $a/2$  were indicated as a zero separation. For 5 and 9 attachment sites, the nearest-neighbor separation histograms are peaked at the designed binding site periodicity. However, for 15 and 29 binding sites, the nearest-neighbor separation histograms are peaked at 2 and 3 periods, respectively. The calculated geometric distributions match the data well for the nanotubes with 5 and 9 attachment

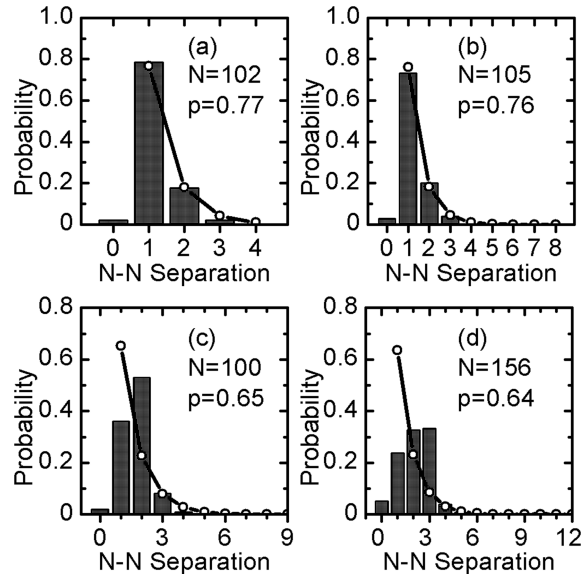


**FIGURE 4.** Histograms (bars) and calculated geometric distributions (lines) for nearest-neighbor (N-N) separation of bound quantum dot pairs for DNA nanotubes with (a) 5, (b) 9, (c) 15, and (d) 29 biotin binding sites. The numbers of separations,  $N$ , measured for each case are provided in the figures, along with the average attachment probabilities,  $p$ . N-N separation of zero indicates two nearest neighbors with a separation less than one-half of a period.

sites, but deviate significantly for the nanotubes with 15 and 29 sites. Thus, the data may indicate that steric hindrance or site bridging reduce the number of quantum dots attached to the nanotubes.

Functionalized DNA origami nanotubes were designed with biotin-labeled staple strands spaced evenly along the axis of the nanotubes. The nanotubes were synthesized and combined with streptavidin-conjugated quantum dots to form nanoparticle arrays with controlled periodicities. AFM images of the synthesized arrays revealed successful attachment of quantum dots at locations along the nanotube axes that corresponded to available biotin binding sites. Statistical analysis of AFM images indicates that binding obstructions establish an upper limit on the yield of nanotubes fully occupied by quantum dots, as indicated by reduced attachment probabilities and deviations from the expected nearest-neighbor distributions for nanotubes with 15 or 29 binding sites. In addition to steric hindrance between quantum dots and quantum dots bridging multiple biotin-labeled staple strands, obstructions may include (1) site poisoning of biotin-labeled staple strands by free streptavidin, (2) biotin-labeled staple strands that are missing their biotin modification, and (3) trapping of tethered biotin inside the DNA nanotube. In addition, a minimum gap distance was measured between two streptavidin-conjugated quantum dots, thereby establishing an important design constraint when fabricating nanoelectronic and nanoplasmonic devices based on DNA origami.

These results provide a powerful and convenient pathway to control nanoparticle patterning, allowing for self-as-

sembled fabrication of nanoscale electronic and photonic devices. Because of the symmetry of DNA origami nanotubes and the nonrepeating sequence of the scaffold strand, it is possible to extend the nanotube functionalization technique to form aperiodic arrays, as well as three-dimensional arrays. Considering there are 170 unique staple strands that can be functionalized by various means at either end, or even within the strand itself, the possibilities for variations are vast. Inclusion of nanoparticles of differing size and/or differing material is within reach and extended networks of functionalized DNA origami nanotubes linked together in two or even three dimensions is plausible.

**Acknowledgment.** The authors are grateful to Dr. Paul W. K. Rothemund for stimulating discussions, Chad Watson for AFM support, Colin Green for acquiring the TEM data included in the Supporting Information S7, and Ross Butler for writing the Perl script included in the Supporting Information S2. This work was supported in part by DARPA Contract No. N66001-01-C-80345, NIH Grant P20 RR016454 from the IN-BRE Program of the National Center for Research Resources, NSF CCF Grant 0855212, and NSF CAREER Grant ECCS-0846415. The TEM work was performed in the Boise State Center for Materials Characterization and supported by the NSF MRI Grant No. DMR-0521315. The AFM work was supported in part by the NSF MRI Grant No. ECCS-0216312.

**Supporting Information Available.** Design schematics and strand sequences for the DNA nanotubes, identification of biotinylated sequences, AFM calibration, and details of AFM, TEM, and statistical image analysis. This material is available free of charge via the Internet at <http://pubs.acs.org>.

## REFERENCES AND NOTES

- (1) Lin, C.; Liu, Y.; Rinker, S.; Yan, H. *ChemPhysChem* **2006**, *7*, 1641–1647.
- (2) Stewart, M. E.; Anderton, C. R.; Thompson, L. B.; Maria, J.; Gray, S. K.; Rogers, J. A.; Nuzzo, R. G. *Chem. Rev.* **2008**, *108*, 494–521.
- (3) Zhao, Y.; Thorkelsson, K.; Mastroianni, A. J.; Schilling, T.; Luther, J. M.; Rancatore, B. J.; Matsunaga, K.; Jinnai, H.; Wu, Y.; Poulsen, D.; Fréchet, J. M. J.; Alivisatos, A. P.; Xu, T. *Nat. Mater.* **2009**, *8*, 979–985.
- (4) Mirkin, C. A.; Letsinger, R. L.; Mucic, R. C.; Storhoff, J. J. *Nature* **1996**, *382*, 607–609.
- (5) Xu, X.; Rosi, N. L.; Wang, Y.; Huo, F.; Mirkin, C. A. *J. Am. Chem. Soc.* **2006**, *128*, 9286–9287.
- (6) Nykypanchuk, D.; Maye, M. M.; van der Lelie, D.; Gang, O. *Nature* **2008**, *451*, 549–552.
- (7) Park, S. Y.; Lytton-Jean, A. K. R.; Lee, B.; Weigand, S.; Schatz, G. C.; Mirkin, C. A. *Nature* **2008**, *451*, 553–556.
- (8) Alivisatos, A. P.; Johnsson, K. P.; Peng, X.; Wilson, T. E.; Loweth, C. J.; Bruchez, M. P., Jr.; Schultz, P. G. *Nature* **1996**, *382*, 609–611.
- (9) Loweth, C. J.; Caldwell, W. B.; Peng, X.; Alivisatos, A. P.; Schultz, P. G. *Angew. Chem., Int. Ed.* **1999**, *38*, 1808–1812.
- (10) Fu, A.; Micheel, C. M.; Cha, J.; Chang, H.; Yang, H.; Alivisatos, A. P. *J. Am. Chem. Soc.* **2004**, *126*, 10832–10833.
- (11) Aldaye, F. A.; Sleiman, H. F. *J. Am. Chem. Soc.* **2007**, *129*, 4130–4131.
- (12) Aldaye, F. A.; Sleiman, H. F. *Angew. Chem., Int. Ed.* **2006**, *45*, 2204–2209.
- (13) Lee, J. H.; Wernette, D. P.; Yigit, M. V.; Liu, J.; Wang, Z.; Lu, Y. *Angew. Chem., Int. Ed.* **2007**, *46*, 9006–9010.
- (14) Niemeyer, C. M.; Bürger, W.; Peplies, J. *Angew. Chem., Int. Ed.* **1998**, *37*, 2265–2268.
- (15) Deng, Z.; Tian, Y.; Lee, S. H.; Ribbe, A. E.; Mao, C. *Angew. Chem., Int. Ed.* **2005**, *44*, 3582–3585.
- (16) Beyer, S.; Nickels, P.; Simmel, F. C. *Nano Lett.* **2005**, *5*, 719–722.
- (17) Seeman, N. C. *Nature* **2003**, *421*, 427–431.
- (18) Seeman, N. C. *Mol. Biotechnol.* **2007**, *37*, 246–257.
- (19) Aldaye, F. A.; Palmer, A. L.; Sleiman, H. F. *Science* **2008**, *321*, 1795–1799.
- (20) Lin, C.; Liu, Y.; Yan, H. *Biochemistry* **2009**, *48*, 1663–1674.
- (21) Chen, J.; Seeman, N. C. *Nature* **1991**, *350*, 631–633.
- (22) Winfree, E.; Liu, F.; Wenzler, L. A.; Seeman, N. C. *Nature* **1998**, *394*, 539–544.
- (23) Shih, W. M.; Quispe, J. D.; Joyce, G. F. *Nature* **2004**, *427*, 618–621.
- (24) Rothemund, P. W. K.; Nkodo, A. E.; Papadakis, N.; Kumar, A.; Fygenson, D. K.; Winfree, E. *J. Am. Chem. Soc.* **2004**, *126*, 16344–16352.
- (25) Rothemund, P. W. K. *Nature* **2006**, *440*, 297–302.
- (26) Kuzuya, A.; Komiyama, M. *Nanoscale* **2010**, *2*, 310–322.
- (27) Shih, W. M.; Lin, C. *Curr. Opin. Struct. Biol.* **2010**, *20*, 276–282.
- (28) Le, J. D.; Pinto, Y.; Seeman, N. C.; Musier-Forsyth, K.; Taton, T. A.; Kiehl, R. A. *Nano Lett.* **2004**, *4*, 2343–2347.
- (29) Zhang, J.; Liu, Y.; Ke, Y.; Yan, H. *Nano Lett.* **2006**, *6*, 248–251.
- (30) Zheng, J.; Constantinou, P. E.; Micheel, C.; Alivisatos, A. P.; Kiehl, R. A.; Seeman, N. C. *Nano Lett.* **2006**, *6*, 1502–1504.
- (31) Sharma, J.; Chhabra, R.; Liu, Y.; Ke, Y.; Yan, H. *Angew. Chem., Int. Ed.* **2006**, *45*, 730–735.
- (32) Sharma, J.; Chhabra, R.; Andersen, C. S.; Gothelf, K. V.; Yan, H.; Liu, Y. *J. Am. Chem. Soc.* **2008**, *130*, 7820–7821.
- (33) Sharma, J.; Ke, Y.; Lin, C.; Chhabra, R.; Wang, Q.; Nangreave, J.; Liu, Y.; Yan, H. *Angew. Chem., Int. Ed.* **2008**, *47*, 5157–5159.
- (34) Hung, A. M.; Micheel, C. M.; Bozano, L. D.; Osterbur, L. W.; Wallraff, G. M.; Cha, J. N. *Nat. Nanotechnol.* **2010**, *5*, 121–126.
- (35) Pal, S.; Deng, Z.; Ding, B.; Yan, H.; Liu, Y. *Angew. Chem., Int. Ed.* **2010**, *49*, 2700–2704.
- (36) Ding, B.; Deng, Z.; Yan, H.; Cabrini, S.; Zuckermann, R. N.; Bokor, J. *J. Am. Chem. Soc.* **2010**, *132*, 3248–3249.
- (37) Sharma, J.; Chhabra, R.; Cheng, A.; Brownell, J.; Liu, Y.; Yan, H. *Science* **2009**, *323*, 112–116.
- (38) Mitchell, G. P.; Mirkin, C. A.; Letsinger, R. L. *J. Am. Chem. Soc.* **1999**, *121*, 8122–8123.
- (39) Mathieu, F.; Liao, S.; Kopatsch, J.; Wang, T.; Mao, C.; Seeman, N. C. *Nano Lett.* **2005**, *5*, 661–665.
- (40) Douglas, S. M.; Chou, J. J.; Shih, W. M. *Proc. Natl. Acad. Sci.* **2007**, *104*, 6644–6648.
- (41) Morris, V. J.; Kirby, A. R.; Gunning, A. P. *Atomic Force Microscopy for Biologists*; Imperial College Press: London, 1999.
- (42) Hertel, T.; Walkup, R. E.; Avouris, P. *Phys. Rev. B* **1998**, *58*, 13870–13873.
- (43) Weisenhorn, A. L.; Khorsandi, M.; Kasas, S.; Gotzos, V.; Butt, H. J. *Nanotechnology* **1993**, *4*, 106–113.
- (44) Weisenhorn, A. L.; Schmitt, F.-J.; Knoll, W.; Hansma, P. K. *Ultramicroscopy* **1992**, *42*–*44*, 1125–1132.
- (45) Perrson, B. N. *J. Chem. Phys. Lett.* **1987**, *141*, 366–368.
- (46) Weisenhorn, A. L.; Drake, B.; Prater, C. B.; Gould, S. A. C.; Hansma, P. K.; Ohnesorge, F.; Egger, M.; Heyn, S. P.; Gaub, H. E. *Biophys. J.* **1990**, *58*, 1251–1258.
- (47) Gould, S. A. C.; Drake, B.; Prater, C. B.; Weisenhorn, A. L.; Manne, S.; Hansma, H. G.; Hansma, P. K.; Massie, J.; Longmire, M.; Elings, V.; Dixon Northern, B.; Mukerjee, B.; Peterson, C. M.; Stoeckenius, W.; Albrecht, T. R.; Quate, C. F. *J. Vac. Sci. Technol. A* **1990**, *8*, 369–373.
- (48) Wilcheck, M.; Bayer, E. A. *Avidin/biotin technology*. *Methods in Enzymology*; Academic Press: San Diego, 1990; Vol. 184.
- (49) Hendrickson, W. A.; Pähler, A.; Smith, J. L.; Satow, Y.; Merritt, E. A.; Phizackerley, R. P. *Proc. Natl. Acad. Sci. U.S.A.* **1989**, *86*, 2190–2194.
- (50) Weber, P. C.; Ohlendorf, D. H.; Wendoloski, J. J.; Salemme, F. R. *Science* **1989**, *243*, 85–88.
- (51) Busse, S.; Scheumann, V.; Menges, B.; Mittler, S. *Biosens. Bioelectron.* **2002**, *17*, 704–710.
- (52) Mendenhall, W.; Scheaffer, R. L. *Mathematical Statistics with Applications*; Duxbury Press: North Scituate, MA, 1972.

